

REVISITING THE ABUNDANCE GRADIENT IN THE MASER HOST GALAXY NGC 4258¹

FABIO BRESOLIN

Institute for Astronomy, 2680 Woodlawn Drive, Honolulu, HI 96822, USA

ABSTRACT

New spectroscopic observations of 36 H II regions in NGC 4258 obtained with the Gemini telescope are combined with existing data from the literature to measure the radial oxygen abundance gradient in this galaxy. The [O III] $\lambda 4363$ auroral line was detected in four of the outermost targets (17 to 22 kpc from the galaxy center), allowing a determination of the electron temperature T_e of the ionized gas. From the use of different calibrations of the R₂₃ abundance indicator an oxygen abundance gradient of approximately -0.012 ± 0.002 dex kpc⁻¹ is derived. Such a shallow gradient, combined with the difference in the distance moduli measured from the Cepheid Period-Luminosity relation by Macri et al. between two distinct fields in NGC 4258, would yield an unrealistically strong effect of metallicity on the Cepheid distances. This strengthens the suggestion that systematic biases might affect the Cepheid distance of the outer field. Evidence for a similar effect in the differential study of M33 by Scowcroft et al. is presented. A revision of the transformation between strong-line and T_e -based abundances in Cepheid-host galaxies is discussed. In the T_e abundance scale, the oxygen abundance of the inner field of NGC 4258 is found to be comparable with the LMC value.

Subject headings: galaxies: abundances — galaxies: ISM — galaxies: individual (NGC 4258)

1. INTRODUCTION

The geometric distance to the spiral galaxy NGC 4258 obtained by Herrnstein et al. (1999, 7.2 ± 0.5 Mpc) from the keplerian motion of water masers in its nucleus represents a cornerstone of the extragalactic distance ladder. The prospect of reducing the uncertainty in the distance from 7% to 3% (Humphreys et al. 2008) opens the possibility of adopting NGC 4258 as a new anchor of the extragalactic distance scale (Riess et al. 2009a), bypassing the use of the LMC, whose distance remains uncertain at the 5-10% level. Moreover, the availability of a geometric distance for a galaxy located well beyond the Local Group offers the opportunity to cross-check the results obtained from primary and secondary distance indicators at distances that are comparable to those of the calibrators of far-reaching standard candles, such as the type Ia supernova peak brightness. Distances to NGC 4258 that are consistent with the geometrically determined one have been obtained from the Cepheid Period-Luminosity ($P-L$) relation (Newman et al. 2001) and the Tip of the Red Giant Branch (TRGB, Mager et al. 2008). From the Cepheids observed with the Hubble Space Telescope (*HST*) by Macri et al. (2006) various authors, using different treatments of the extinction and metallicity corrections, together with the adoption of different $P-L$ relations, have obtained distance moduli that differ at the 0.1 mag level, but that are still compatible, within the reported uncertainties, with the maser distance (An et al. 2007; van Leeuwen et al. 2007; Benedict et al. 2007; Turner 2010).

The effect of metallicity on the Cepheid $P-L$ relation is a crucial but still debated issue. A persistent discrepancy between theoretical predictions from pulsation models

(Fiorentino et al. 2007; Bono et al. 2008) and empirical determinations (Macri et al. 2006; Scowcroft et al. 2009) lingers on. In the *HST* Key Project (Freedman et al. 2001) a metallicity correction factor $\gamma = \delta\mu_0 / \delta \log Z = -0.20$ mag dex⁻¹ was applied to the galaxy distance moduli, in the sense of making them larger for metallicities exceeding the LMC value. The estimated contribution of the metallicity to the present 5% uncertainty on the Hubble constant H_0 is about 2.5% (Freedman & Madore 2010). Current efforts striving for an accuracy better than 5% on H_0 attempt to circumvent this issue by selecting galaxies with similar metal content (Riess et al. 2009b).

Given the importance of NGC 4258 in current investigations of the extragalactic distance scale, in this paper the oxygen abundance of its interstellar medium (a proxy for the Cepheid metallicity) is revisited. One of the initial goals of this new study was to determine oxygen abundances from direct electron temperature (T_e) determinations in H II regions. This requires deep integrations with large aperture telescopes, in order to detect the weak [O III] $\lambda 4363$ auroral line, which provides, in combination with the much stronger [O III] $\lambda \lambda 4959, 5007$ nebular lines, the crucial temperature diagnostic for ionized nebulae. Despite the fact that NGC 4258 has been the subject of previous abundance studies based on its H II region population, the $\lambda 4363$ line has remained unobserved until the present time. Secondly, it was felt that an investigation based on new spectroscopic data was warranted in order to verify the recent determination of the metallicity effect on the $P-L$ relation obtained by Macri et al. (2006) from a differential study of Cepheids located in two fields at different distances from the galaxy center (and therefore different metal content). This study adopted metallicities determined from the calibration of the R₂₃ strong-line indicator by Zaritsky et al. (1994), applied to H II region emission-line data obtained by the same authors and Oey & Kennicutt (1993). However, a recent reanalysis of these data by Bono et al. (2008) suggested that the abundance gradient might need to be revised. Lastly, during the course of this work some inconsistencies were found in the T_e -based abundance scale adopted

¹ Based on observations obtained at the Gemini Observatory, which is operated by the Association of Universities for Research in Astronomy, Inc., under a cooperative agreement with the NSF on behalf of the Gemini partnership: the National Science Foundation (United States), the Science and Technology Facilities Council (United Kingdom), the National Research Council (Canada), CONICYT (Chile), the Australian Research Council (Australia), Ministério da Ciência e Tecnologia (Brazil) and Ministerio de Ciencia, Tecnología e Innovación Productiva (Argentina).

in several published studies of extragalactic Cepheids (Sakai et al. 2004; Saha et al. 2006), and these will also be addressed for the benefit of future studies.

It is important to keep in mind that the determination of extragalactic chemical abundances from nebular spectroscopy is still afflicted by large systematic uncertainties, despite the maturity of the field (see Bresolin 2008 for a recent review). A well-established discrepancy exists between abundances obtained from the classical, *direct* T_e -based method (Menzel et al. 1941) and the theoretical predictions of photoionization model grids (McGaugh 1991). In addition, the study of metal *recombination* lines provides oxygen abundances that lie between the direct (from *collisionally excited* lines) and the theoretical values (García-Rojas et al. 2007). Generally, it is believed that differential analysis methods are unaffected by these systematic differences. However, in the case of the T_e vs. strong-line methods in the high metallicity regime (around the solar oxygen abundance $12 + \log(\text{O}/\text{H})_\odot = 8.69$, Asplund et al. 2009) this conclusion is still based on a limited number of experimental data points.

2. OBSERVATIONS AND DATA REDUCTION

New spectra of H II regions in NGC 4258 were obtained with the Gemini Multi-Object Spectrograph (GMOS, Hook et al. 2004) at the Gemini North facility on Mauna Kea. The targets were selected from H α narrow-band images of two 5.5×5.5 GMOS fields, centered approximately 2.3 NW and 6.5 SE of the center of the galaxy, obtained between January and March 2010. The spectroscopic data were acquired in queue mode between March and June 2010, using two multi-object masks, one per field, with 1.5 -wide slitlets. The seeing conditions were around 0.8 during the observations of the NW field, and around 0.5 for the SE field. In order to minimize the effects of the atmospheric differential refraction the data were acquired at airmasses smaller than 1.20. Three 3000 s exposures were secured for each of the two fields using the B600 grating, which provided spectra covering at least the 3500–5100 Å wavelength range at a spectral resolution of ~ 5.5 Å. For some of the targets, depending on their spatial distribution, the spectral coverage extended up to ~ 5900 Å.

IRAF² routines contained in the `gemini/gmos` package were used for cosmic ray rejection, electronic bias subtraction, flat field correction and wavelength calibration of the raw data frames. Observations of the spectrophotometric standard Feige 34 yielded the flux calibration. Thanks to the similarity in airmass and atmospheric conditions between the three different frames obtained for each individual target, the emission line intensities of the single extracted spectra are very consistent with each other. The working version of the spectra was then obtained by averaging the three spectra corresponding to each individual slit.

The final H II region sample comprises 36 objects, equally divided between the NW and the SE fields. Their celestial coordinates are summarized in Table 2 (where objects are listed in order of decreasing declination), together with their galactocentric distances in kpc, deprojected using the geometric parameters in Table 1. Fig. 1 shows the location of the spectroscopic targets on an H α image of NGC 4258 (circles numbered 1 to 36). It can be seen that all but three of the objects

Table 1
NGC 4258: adopted parameters

Parameter	Value
R.A. (J2000.0)	12 18 57.50 ^a
Decl. (J2000.0)	47 18 14.3 ^a
Morphological type	SAB(s)bc ^b
Distance	7.2 Mpc ^c
R_{25}	9.31 ^b (19.50 kpc)
Inclination	72° ^d
Position angle of major axis	150° ^d
B_T^0	8.53 ^b
M_B^0	−20.76

References. — (a) Herrnstein et al. (2005); (b) de Vaucouleurs et al. (1991); (c) Herrnstein et al. (1999); (d) van Albada (1980).

lie within the R_{25} radius (i.e. within the ellipse in the figure). The H II regions observed in the NW field sample a portion of the northern inner spiral arm of the galaxy, together with a few objects close to the galaxy center and in the northern outer arm. The H II regions in the SE field are mostly located in the southern outer arm (a description of the complex spiral morphology of NGC 4258 is given by Courtes et al. 1993).

2.1. Line fluxes and comparison with previous work

The emission line intensities were measured with the `splot` program in IRAF by integrating the fluxes under the line profiles. The metal lines [O II] $\lambda 3727$, [O III] $\lambda \lambda 4959, 5007$ and the H β , H γ Balmer lines were present in the spectra of all the 36 targets in Table 2. The weaker [Ne III] $\lambda 3868$ and H δ lines were measured in 19 and 33 H II regions, respectively. The line intensities were corrected for interstellar reddening by assuming a case B intrinsic H γ /H β ratio of 0.47 at $T_e = 10^4$ K and the Seaton (1979) reddening law. The resulting reddening-corrected emission lines, normalized to H $\beta = 100$, are presented in Table 3. The line errors reported in the table account for uncertainties in the flat fielding, the flux calibration, the positioning of the continuum level around each line and the extinction coefficient $c(\text{H}\beta)$.

A few of the brightest objects in the sample have already been studied spectroscopically by other authors, in particular six targets are in common with Oey & Kennicutt (1993), Zaritsky et al. (1994) and Bresolin et al. (1999), and these are identified in column 5 of Table 2. Fig. 2 compares the [O II] $\lambda 3727$ (circles) and [O III] $\lambda \lambda 4959, 5007$ (triangles) line fluxes measured in the present study with those measured by these other authors. The agreement is found to be excellent: the mean ratio between the two sets is 1.01 ± 0.04 .

3. OXYGEN ABUNDANCES

3.1. Electron temperatures and direct abundances

One of the goals of this new spectroscopic investigation of NGC 4258 was to measure, for as many H II regions as possible, the electron temperature of the nebular gas via the standard method that involves the detection of the [O III] $\lambda 4363$ auroral line. No previous detection of this line has been reported in the literature for NGC 4258. In this new study, the $\lambda 4363$ line was measured for four H II regions (numbers 24, 30, 34 and 36 in Table 2), all of them located at large galactocentric distances and along the southern outer spiral arm. The `nebular` package in IRAF was used to derive electron temperatures (adopting an electron density of 10^2 cm^{-3} and the atomic parameters used by Bresolin et al. 2009), and the O⁺,

² IRAF is distributed by the National Optical Astronomy Observatories, which are operated by the Association of Universities for Research in Astronomy, Inc., under cooperative agreement with the National Science Foundation.

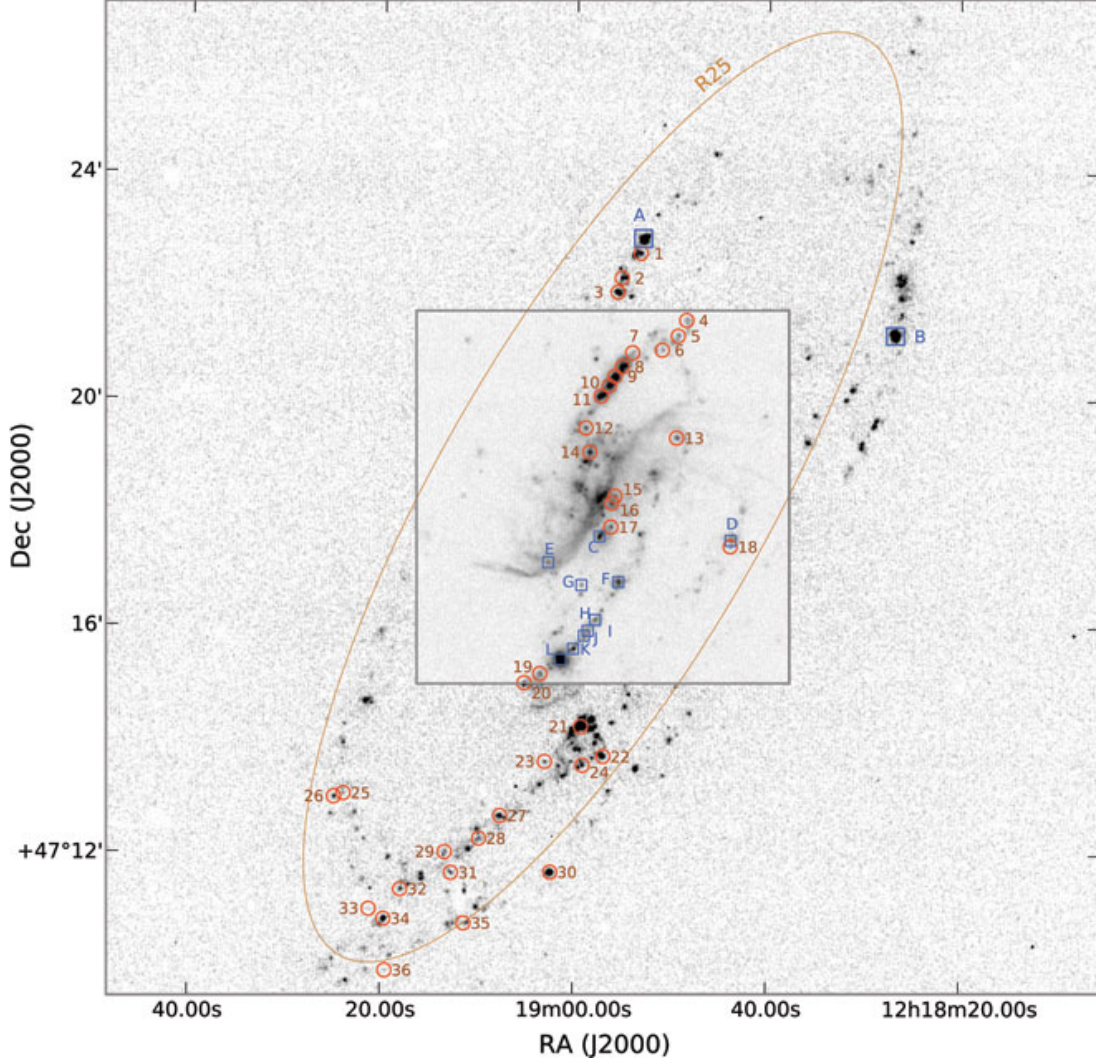


Figure 1. Location of the H II regions studied in this work on a narrow-band H α image of NGC 4258 (courtesy L. van Zee). The H II regions are numbered in order of decreasing declination. Letters identify objects drawn from the literature. The ellipse represents the location of the projected R_{25} radius ($R_{25} = 9''.31$). The inner and outer parts of the galaxy are shown with different stretchings, in order to facilitate the identification of the targets.

O $^{++}$ ionic abundances. The resulting temperatures and total O/H abundance ratios are presented in Table 4. The electron temperatures and the $12 + \log(\text{O}/\text{H})$ abundances are remarkably similar among the four targets, with mean values of 11400 K and 8.20, respectively.

3.2. Strong-line abundances

For the majority of the H II regions in our sample we need to resort to the use of strong-line abundance indicators, since the auroral lines remain undetected. The difficulties and potential pitfalls of these methods have been described at length in the literature (see Bresolin et al. 2009 for a recent overview) and will not be repeated here. In brief, with these methods the value of the oxygen abundance is related to the strength of metal lines in the optical nebular spectra either via an empirical calibration obtained from H II regions with auroral line detections ('empirical' method) or via the results of theoretical photoionization models. The abundances derived from the different procedures and calibrations vary in a systematic way by large factors, with empirical abundances typically occupying the low end of the range. While this situation is cur-

rently unexplained, relative abundances are generally considered to be rather robust. Investigations of additional present-day abundance indicators in galaxies (e.g. blue supergiants, Kudritzki et al. 2008) are presently being carried out, with the goal of establishing the reliability of the absolute nebular abundances obtained by the different calibrations. Recent work in the nearby galaxies NGC 300 and M33 has shown that a good agreement is obtained between the supergiant and H II region abundances when the latter are based on the direct, [O III] $\lambda 4363$ -based method (Bresolin et al. 2009, 2010). For this reason, it is important to be able to anchor the strong-line abundances obtained in more distant galaxies to the values provided by the detection of the [O III] $\lambda 4363$ auroral line, as done in the present investigation of NGC 4258. While relative abundance determinations seem to be, to first order, unaffected by the choice of technique used to measure them (but see last paragraph of Sec. 6.1), it is also true that it is important to establish the absolute nebular abundances in order to constrain the chemical evolutionary status of star-forming galaxies, a fact that is often overlooked.

For this study of NGC 4258 it was decided to investi-

Table 2
Observed H II region sample

ID	R.A.	Decl.	R	other ID
(1)	(J2000.0)	(J2000.0)	(kpc)	(5)
1.....	12 18 53.31	47 22 35.5	13.66	
2.....	12 18 55.26	47 22 09.5	13.36	
3.....	12 18 55.69	47 21 54.3	12.70	
4.....	12 18 48.52	47 21 24.8	7.58	
5.....	12 18 49.39	47 21 08.2	6.92	
6.....	12 18 51.05	47 20 53.3	6.48	
7.....	12 18 54.13	47 20 50.3	7.62	
8.....	12 18 55.20	47 20 35.5	7.36	34C, (−032 + 141), B3
9.....	12 18 55.94	47 20 25.5	7.23	39C, (−025 + 130), B4
10.....	12 18 56.55	47 20 15.2	7.01	44C, (−019 + 121), B5
11.....	12 18 57.37	47 20 04.3	6.94	52C, (−010 + 110)
12.....	12 18 58.93	47 19 30.6	6.09	61C
13.....	12 18 49.51	47 19 20.4	5.43	18C
14.....	12 18 58.52	47 19 05.0	4.10	56C
15.....	12 18 55.87	47 18 18.7	1.43	38C
16.....	12 18 56.19	47 18 11.2	1.48	42C
17.....	12 18 56.28	47 17 46.0	2.89	43C
18.....	12 18 43.86	47 17 25.7	16.35	3C
19.....	12 19 03.56	47 15 10.6	7.93	82Ca, (+039 − 185)
20.....	12 19 05.18	47 15 00.8	7.93	83Ca
21.....	12 18 59.29	47 14 14.8	13.97	7Sa
22.....	12 18 56.96	47 13 43.3	17.79	1Sa
23.....	12 19 03.01	47 13 37.6	13.79	
24.....	12 18 59.09	47 13 33.8	16.74	
25.....	12 19 23.88	47 13 03.2	16.55	29S
26.....	12 19 24.87	47 12 59.6	17.21	32S
27.....	12 19 07.63	47 12 40.2	14.79	2S
28.....	12 19 09.78	47 12 16.0	15.28	4S
29.....	12 19 13.34	47 12 01.6	15.04	
30.....	12 19 02.38	47 11 40.7	21.56	ZKH 8
31.....	12 19 12.68	47 11 39.6	16.30	
32.....	12 19 17.94	47 11 22.0	16.36	
33.....	12 19 21.18	47 11 01.0	17.33	
34.....	12 19 19.65	47 10 50.6	17.61	16S
35.....	12 19 11.33	47 10 46.4	19.72	
36.....	12 19 19.49	47 09 56.0	19.97	

Note. — Units of right ascension are hours, minutes and seconds, and units of declination are degrees, arcminutes and arcseconds. Col. (1): H II region identification. Col. (2): Right ascension. Col. (3): Declination. Col. (4): Deprojected galactocentric distance in kpc. Col. (5): Main identification from Courtes et al. (1993), with additional objects from Zaritsky et al. (1994, = ZKH), Oey & Kennicutt (1993, coordinates in brackets) and Bresolin et al. (1999, = B).

gate the abundances obtained from the strong-line indicator $R_{23} = ([\text{O II}] \lambda 3727 + [\text{O III}] \lambda \lambda 4959, 5007)/H\beta$ (Pagel et al. 1979). Two different calibrations are adopted: the one by McGaugh (1991, in the analytical form given by Kuzio de Naray et al. 2004), which is based on a grid of photoionization models, and the one by Pilyugin & Thuan (2005). The latter was selected as an alternative because it is essentially calibrated from auroral line-based abundances, and thus it should provide results that are in agreement with those obtained from the $[\text{O III}] \lambda 4363$ detections. Both calibrations account for the excitation of the ionized gas, via the parameters $y = \log(\text{O3}/\text{O2})$ and $P = \text{O3}/(\text{O3} + \text{O2})$, respectively, where $\text{O3} = [\text{O III}] \lambda \lambda 4959, 5007$ and $\text{O2} = [\text{O II}] \lambda 3727$.

The double-valued nature of R_{23} represents a major source of uncertainty when it is difficult to ascertain whether the targets fall onto the upper (high O/H) or lower (low O/H) branch of the indicator. This issue is commonly resolved by considering emission line ratios that are monotonic with O/H, such as $[\text{N II}]/H\alpha$ and $[\text{N II}]/[\text{O II}]$. Our spectra do not cover the region around $H\alpha$, and therefore we can neither use indicators based on the strength of the $[\text{N II}] \lambda 6583$ line

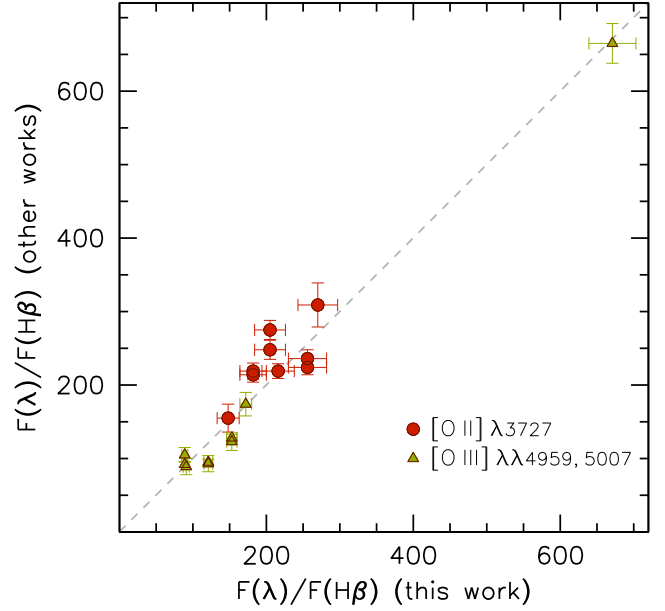


Figure 2. Comparison between the $[\text{O II}] \lambda 3727$ and $[\text{O III}] \lambda \lambda 4959, 5007$ reddening-corrected fluxes measured in this work and in previous publications. The dashed line represents the one-to-one line.

(e.g. $N2 = \log([\text{N II}]/H\alpha)$, Pettini & Pagel 2004), nor use this information to select the appropriate R_{23} branch. Nevertheless, it is possible to select the upper branch calibration for the full sample with high confidence, based on the following considerations:

(a) Fig. 3 shows the relation between R_{23} and O/H for H II regions in a number of spiral and irregular galaxies, for which the oxygen abundance was derived from high-quality measurements of the $[\text{O III}] \lambda 4363$ line and extracted from the following references:

NGC 300:	Bresolin et al. (2009)
M101:	Kennicutt et al. (2003)
NGC 2403:	Garnett et al. (1997)
	Esteban et al. (2009)
M33:	Bresolin et al. (2010)
	Esteban et al. (2009)
IC 1613:	Bresolin et al. (2006)
H II galaxies:	Izotov et al. (1994)
	Guseva et al. (2009)
M31, NGC 2363, NGC 1741	Esteban et al. (2009)
NGC 4395, NGC 4861	

In selecting the spiral galaxy sample preference was given to investigations carried out by the author and his collaborators, in order to ensure consistency in the reduction and data analysis procedures. The data plotted in Fig. 3 clearly delineate the two R_{23} branches, with the turnover point located around $12 + \log(\text{O}/\text{H}) = 8.0$. Most of the H II galaxies shown here fall below the turnover point and lie on the lower branch. Virtually all of the H II regions in spiral galaxies are located on the upper branch (the notable exception is represented by region SDH 323 in M101, which lies at a very large distance from the galaxy center). The lines drawn in Fig. 3 are polynomial fits to the data, for $12 + \log(\text{O}/\text{H})$ above and below the turnover point, and are shown to guide the eye in identifying the two R_{23} branches. The four squares in Fig. 3 represent

Table 3
Reddening-corrected line fluxes and strong-line oxygen abundances

ID	[O II] 3727	[Ne III] 3868	H I 4101	[O III] 4959	[O III] 5007	log(R ₂₃)	F(H β) (erg s ⁻¹ cm ⁻²)	c(H β) (mag)	12 + log(O/H)	
(1)	(2)	(3)	(4)	(5)	(6)	(7)	(8)	(9)	M91 (10)	P05 (11)
1.....	273 ± 28	13.9 ± 1.8	23 ± 2	63 ± 4	190 ± 11	0.72 ± 0.04	3.3 × 10 ⁻¹⁵	0.23	8.67 ± 0.04	8.35 ± 0.05
2.....	263 ± 27	12.5 ± 1.7	26 ± 2	60 ± 4	178 ± 11	0.70 ± 0.04	3.2 × 10 ⁻¹⁵	0.18	8.69 ± 0.04	8.37 ± 0.05
3.....	290 ± 29	10.5 ± 1.6	26 ± 2	58 ± 3	166 ± 10	0.71 ± 0.04	3.3 × 10 ⁻¹⁵	0.12	8.67 ± 0.04	8.33 ± 0.05
4.....	248 ± 25	...	26 ± 2	44 ± 3	130 ± 8	0.62 ± 0.04	1.7 × 10 ⁻¹⁵	0.28	8.75 ± 0.03	8.40 ± 0.05
5.....	249 ± 25	...	25 ± 2	28 ± 2	80 ± 5	0.55 ± 0.04	4.3 × 10 ⁻¹⁵	0.42	8.81 ± 0.03	8.36 ± 0.05
6.....	247 ± 25	...	20 ± 2	21 ± 1	65 ± 4	0.52 ± 0.04	2.6 × 10 ⁻¹⁵	0.17	8.82 ± 0.03	8.34 ± 0.05
7.....	219 ± 22	...	26 ± 2	14 ± 1	42 ± 3	0.44 ± 0.04	2.1 × 10 ⁻¹⁵	0.33	8.88 ± 0.03	8.34 ± 0.04
8.....	256 ± 26	2.9 ± 0.4	29 ± 2	22 ± 1	67 ± 4	0.54 ± 0.04	2.6 × 10 ⁻¹⁴	0.41	8.81 ± 0.03	8.33 ± 0.05
9.....	182 ± 18	3.6 ± 0.4	24 ± 2	38 ± 2	115 ± 7	0.53 ± 0.04	5.5 × 10 ⁻¹⁴	0.27	8.84 ± 0.03	8.53 ± 0.04
10.....	205 ± 21	2.8 ± 0.5	24 ± 3	30 ± 2	91 ± 5	0.51 ± 0.04	1.7 × 10 ⁻¹⁴	0.50	8.84 ± 0.03	8.46 ± 0.04
11.....	216 ± 22	3.7 ± 0.9	25 ± 2	23 ± 1	68 ± 4	0.49 ± 0.04	1.3 × 10 ⁻¹⁴	0.20	8.86 ± 0.03	8.41 ± 0.04
12.....	189 ± 19	6.7 ± 1.7	24 ± 2	69 ± 4	205 ± 12	0.67 ± 0.03	4.7 × 10 ⁻¹⁵	0.44	8.74 ± 0.03	8.49 ± 0.04
13.....	206 ± 21	6.1 ± 0.9	27 ± 2	40 ± 2	119 ± 7	0.56 ± 0.04	7.8 × 10 ⁻¹⁵	0.05	8.81 ± 0.03	8.48 ± 0.04
14.....	234 ± 24	...	24 ± 2	29 ± 2	87 ± 5	0.54 ± 0.04	6.1 × 10 ⁻¹⁵	0.35	8.81 ± 0.03	8.40 ± 0.04
15.....	199 ± 20	...	25 ± 2	24 ± 1	72 ± 4	0.47 ± 0.04	5.1 × 10 ⁻¹⁵	0.00	8.87 ± 0.03	8.46 ± 0.04
16.....	243 ± 24	7.3 ± 1.0	26 ± 2	50 ± 3	148 ± 9	0.64 ± 0.04	7.9 × 10 ⁻¹⁵	0.37	8.74 ± 0.03	8.41 ± 0.05
17.....	222 ± 22	6.5 ± 0.8	26 ± 2	44 ± 3	128 ± 8	0.59 ± 0.04	6.5 × 10 ⁻¹⁵	0.16	8.78 ± 0.03	8.45 ± 0.04
18.....	246 ± 25	4.9 ± 0.8	28 ± 2	38 ± 2	112 ± 7	0.60 ± 0.04	4.2 × 10 ⁻¹⁵	0.00	8.78 ± 0.03	8.40 ± 0.05
19.....	270 ± 27	8.7 ± 1.1	26 ± 2	43 ± 2	129 ± 8	0.64 ± 0.04	5.5 × 10 ⁻¹⁵	0.39	8.73 ± 0.04	8.36 ± 0.05
20.....	329 ± 33	23.6 ± 2.3	30 ± 2	74 ± 4	223 ± 13	0.80 ± 0.04	9.0 × 10 ⁻¹⁵	0.90	8.58 ± 0.05	8.25 ± 0.06
21.....	194 ± 20	13.9 ± 2.5	26 ± 3	56 ± 3	176 ± 10	0.63 ± 0.03	1.9 × 10 ⁻¹⁵	0.66	8.76 ± 0.03	8.50 ± 0.04
22.....	274 ± 28	...	26 ± 2	26 ± 2	74 ± 4	0.57 ± 0.04	2.1 × 10 ⁻¹⁵	0.20	8.78 ± 0.04	8.30 ± 0.05
23.....	422 ± 44	...	24 ± 4	48 ± 3	142 ± 8	0.79 ± 0.04	1.0 × 10 ⁻¹⁵	1.14	8.56 ± 0.05	8.09 ± 0.07
24.....	213 ± 22	47.4 ± 4.5	25 ± 2	157 ± 9	465 ± 28	0.92 ± 0.03	1.6 × 10 ⁻¹⁵	0.26	8.50 ± 0.04	8.29 ± 0.05
25.....	113 ± 13	...	23 ± 3	104 ± 6	303 ± 18	0.71 ± 0.03	6.0 × 10 ⁻¹⁶	0.35	8.73 ± 0.03	8.54 ± 0.03
26.....	374 ± 39	29 ± 2	91 ± 5	0.70 ± 0.04	8.2 × 10 ⁻¹⁶	0.35	8.65 ± 0.05	8.13 ± 0.06
27.....	355 ± 36	...	27 ± 3	19 ± 1	58 ± 3	0.64 ± 0.04	1.5 × 10 ⁻¹⁵	0.43	8.71 ± 0.05	8.11 ± 0.06
28.....	286 ± 31	...	25 ± 4	57 ± 4	171 ± 10	0.71 ± 0.04	3.9 × 10 ⁻¹⁶	0.12	8.67 ± 0.04	8.33 ± 0.06
29.....	337 ± 35	...	30 ± 4	56 ± 3	167 ± 10	0.75 ± 0.04	6.2 × 10 ⁻¹⁶	0.63	8.62 ± 0.05	8.24 ± 0.06
30.....	149 ± 15	47.2 ± 4.5	29 ± 2	169 ± 10	501 ± 30	0.91 ± 0.03	1.3 × 10 ⁻¹⁴	0.28	8.54 ± 0.04	8.34 ± 0.04
31.....	314 ± 32	...	26 ± 3	76 ± 4	231 ± 14	0.79 ± 0.04	7.8 × 10 ⁻¹⁶	0.08	8.59 ± 0.04	8.28 ± 0.06
32.....	287 ± 30	14 ± 1	42 ± 3	0.54 ± 0.04	8.5 × 10 ⁻¹⁶	0.07	8.80 ± 0.04	8.20 ± 0.05
33.....	241 ± 27	118 ± 7	353 ± 21	0.85 ± 0.03	3.2 × 10 ⁻¹⁶	0.08	8.56 ± 0.04	8.33 ± 0.05
34.....	314 ± 32	18.8 ± 1.9	26 ± 2	80 ± 5	237 ± 14	0.80 ± 0.03	5.5 × 10 ⁻¹⁵	0.20	8.58 ± 0.04	8.28 ± 0.06
35.....	326 ± 33	...	23 ± 3	52 ± 3	157 ± 9	0.73 ± 0.04	8.0 × 10 ⁻¹⁶	0.00	8.64 ± 0.04	8.26 ± 0.06
36.....	193 ± 20	32.9 ± 4.3	25 ± 2	169 ± 10	492 ± 29	0.93 ± 0.03	6.0 × 10 ⁻¹⁶	0.00	8.50 ± 0.04	8.29 ± 0.05

Note. — The line fluxes are in units of $H\beta = 100$. $F(H\beta)$ in column (8) is the measured $H\beta$ flux, uncorrected for extinction. The oxygen abundances in columns (10) and (11) are obtained with the R_{23} calibrations by McGaugh (1991, = M91) and Pilyugin & Thuan (2005, = P05), respectively.

Table 4
Direct method abundances

ID	[O III] λ 4363	T_e (K)	12 + log(O/H)
(1)	(2)	(3)	(4)
24.....	4.5 ± 0.7	11350 ± 850	8.23 ± 0.10
30.....	5.0 ± 0.4	11490 ± 530	8.19 ± 0.06
34.....	1.9 ± 0.2	10640 ± 510	8.23 ± 0.07
36.....	5.6 ± 1.0	12030 ± 1050	8.16 ± 0.11

Note. — The reddening-corrected intensity of [O III] λ 4363 in column 2 is in units of $H\beta = 100$.

the H II regions in NGC 4258 for which a direct abundance was obtained (see Table 4). It can be seen that these objects are placed on the upper branch. Considering the fact that these H II regions are among the most distant from the center of NGC 4258, and that galactic abundance gradients are always measured to be monotonic, with abundances increasing toward the central regions, this result strongly suggests that the remaining H II regions in this galaxy (which have

smaller R_{23} values, as shown in column 7 of Table 3) have larger abundances, and should therefore also be placed on the upper branch.

(b) all of the H II regions without [O III] λ 4363 detections have $\log(R_{23}) < 0.80$, i.e. significantly lower than the turnaround point where the two branches intersect. From Fig. 3 we can infer that misplacing a lower branch object onto the upper branch would increase the estimated O/H ratio by approximately 0.5 dex or more. This would easily show up in a plot of the galactocentric abundance gradient, under the assumption that the gradient is monotonic and without abrupt discontinuities. If we assume upper branch objects only for our sample, the gradient in NGC 4258 behaves ‘normally’. If instead we assume that some of the objects at high R_{23} values belong to the lower branch, we obtain very large discontinuities in the abundance gradient, which can be reasonably excluded for H II regions located within the optical boundaries of normal galaxies.

(c) For four of the targets (4, 5, 13 and 34 in Table 3) the auroral [N II] λ 5755 line was within the covered wavelength

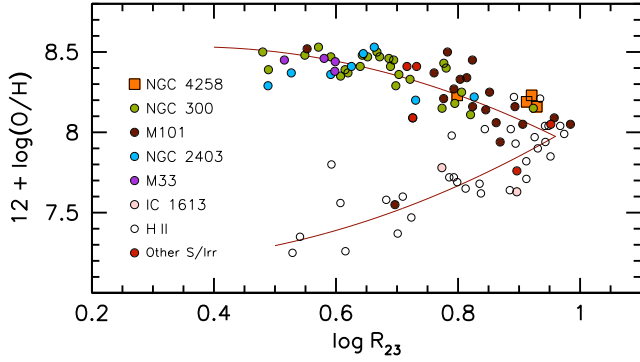


Figure 3. $\log(R_{23})$ vs. $12 + \log(O/H)$ for a sample of extragalactic H II regions drawn from the literature. The oxygen abundances were all derived using the direct method, i.e. using the [O III] $\lambda 4363$ auroral lines. The different symbols correspond to the galaxies identified in the legend. References for the data are given in the text. The four H II regions in NGC 4258 with a measured [O III] $\lambda 4363$ line are shown by the orange squares. The curves represent the upper and lower branch of the R_{23} indicator, obtained from a polynomial fit to the data.

range and sufficiently strong to allow a good measurement of its intensity. This line, in combination with the much stronger [N II] $\lambda 6583$, can be used to measure the electron temperature in the low-ionization zone of an H II region, in order to determine, for example, the N^+ and O^+ ionic abundances (Bresolin et al. 2004). Here we can use it to infer the strength of the [N II] $\lambda 6583$ line, making a reasonable assumption for the value of the electron temperature. Then, the $N2 = \log([N II] \lambda 6583 / H\alpha)$ index can be used in the traditional way to assign the objects to the lower or upper R_{23} branch. For example, assuming $T_e = 10,000$ K ($T_e = 10,600$ K for object 34, as derived from the [O III] $\lambda 4363$ line), from the `temden` routine in IRAF we obtain $N2 = -0.72 \pm 0.08, -0.61 \pm 0.05, -0.77 \pm 0.05$, and -0.94 ± 0.06 for the four objects, respectively. It is generally adopted that for $N2 > -1.2$, the upper branch solution of R_{23} should be preferred (e.g. Kewley & Ellison 2008). The boundary between upper and lower branch could be safely lowered to $N2 \simeq -1.4$, if we consider that the upper and lower branches intersect around $12 + \log(O/H) = 8.0$, when the abundances are determined empirically (see Fig. 3). A plot of empirical ([O III] $\lambda 4363$ -based) abundances vs. $N2$ shows that this value corresponds to $N2 = -1.5$ (Pettini & Pagel 2004). In any case, the $N2$ values we estimated above place the targets safely in the upper branch. Only once we approach a T_e value of 14,000 K would the $N2$ estimates be below -1.2 . However, such high temperatures can be reasonably excluded by pointing out that the directly measured electron temperature values, approximately between 11,000 K and 12,000 K, are found for objects located at the largest galactocentric distances in NGC 4258, while the electron temperature is expected to decrease towards smaller radii (Bresolin et al. 2009).

In conclusion, there are strong arguments to favor the selection of upper branch calibrations of R_{23} for the whole H II region sample analyzed in this paper.

4. THE OXYGEN ABUNDANCE GRADIENT IN NGC 4258

The adoption of the R_{23} upper branch, justified in the previous section, yields the oxygen abundances presented in columns (10) and (11) of Table 3, obtained with the McGaugh (1991, = M91) and Pilyugin & Thuan (2005, = P05) calibrations, respectively. For the derivation of the abundance gradi-

Table 5
Additional H II regions from the literature

ID	R.A.	Decl.	R	other ID
(1)	(2)	(3)	(4)	(5)
A	12 18 53.062	47 22 51.23	14.48	ZKH 9
B	12 18 26.791	47 21 09.23	23.30	ZKH 1, 5NA, B1 OK (-318+183)
C	12 18 57.445	47 17 35.83	2.51	ZKH 6 OK (-014-038)
D	12 18 43.814	47 17 32.21	16.04	ZKH 2, B2 OK (-152-037)
E	12 19 02.768	47 17 08.26	3.30	ZKH 5
F	12 18 55.470	47 16 47.82	7.27	OK (-035-086)
G	12 18 59.308	47 16 44.46	4.47	ZKH 7
H	12 18 57.856	47 16 07.69	7.84	54C
I	12 18 58.614	47 15 56.09	8.00	58C
J	12 18 58.997	47 15 50.89	8.06	59C
				OK (-005-150)
K	12 19 00.116	47 15 36.95	8.17	69C
L	12 19 01.438	47 15 25.66	8.07	OK (+024-170), 74C

Note. — Units of right ascension are hours, minutes and seconds, and units of declination are degrees, arcminutes and arcseconds. Col. (1): H II region identification. Col. (2): Right Ascension. Col. (3): Declination. Col. (4): Galactocentric distance in kpc. Col. (5): Identification from Oey & Kennicutt (1993, = OK), Zaritsky et al. (1994, = ZKH), Bresolin et al. (1999, = B) and Courtes et al. (1993, studied by Díaz et al. 2000).

ent the line fluxes of 12 additional H II regions published by Oey & Kennicutt (1993), Zaritsky et al. (1994) and Díaz et al. (2000) were added to our sample. These objects are identified with letters in Fig. 1, and their positions and galactocentric distances can be found in Table 5. When the same target was observed by these authors, the average [O II] and [O III] line fluxes were computed. For objects from our sample that are in common with these authors (see Table 2 and Fig. 2), only our new measurements were considered.

The galactocentric O/H gradient in NGC 4258 is presented in Fig. 4. In this plot abundances for the Gemini H II region sample calculated with the M91 and P05 R_{23} calibrations are shown as full squares and full triangles, respectively. Open symbols (squares and triangles for M91 and P05, respectively) are used for the H II regions extracted from the literature. In the case of the abundances based on the P05 method objects with values of the excitation $P < 0.3$ were removed, since the calibration provided by P05 only covers $P > 0.3$, and we found that for objects with smaller excitation values the abundances could be overestimated.

For the calculation of the radial abundance gradient a least-squares fit that accounts for errors in both coordinates (abundance and radius) was carried out. Because of the high inclination of the disk of NGC 4258 relative to the line of sight (78°), even a relatively small uncertainty in this angle can result into an appreciable error in the computed deprojected distances, especially for objects located near the minor axis. The source of the geometric parameters of the disk of NGC 4258 adopted here, van Albada (1980), does not explicitly provide uncertainty estimates, but implies that the errors in the radio-determined position angle of the major axis and inclination are much smaller than 2° and 1° , respectively. A 1° uncertainty was assumed for both angles. We also accounted for an astrometric uncertainty of $0''.4$ in the H II region positions. The resulting error in the galactocentric distance reaches a maximum value of 6%, but for the majority of the targets it is on the order of 1-2%.

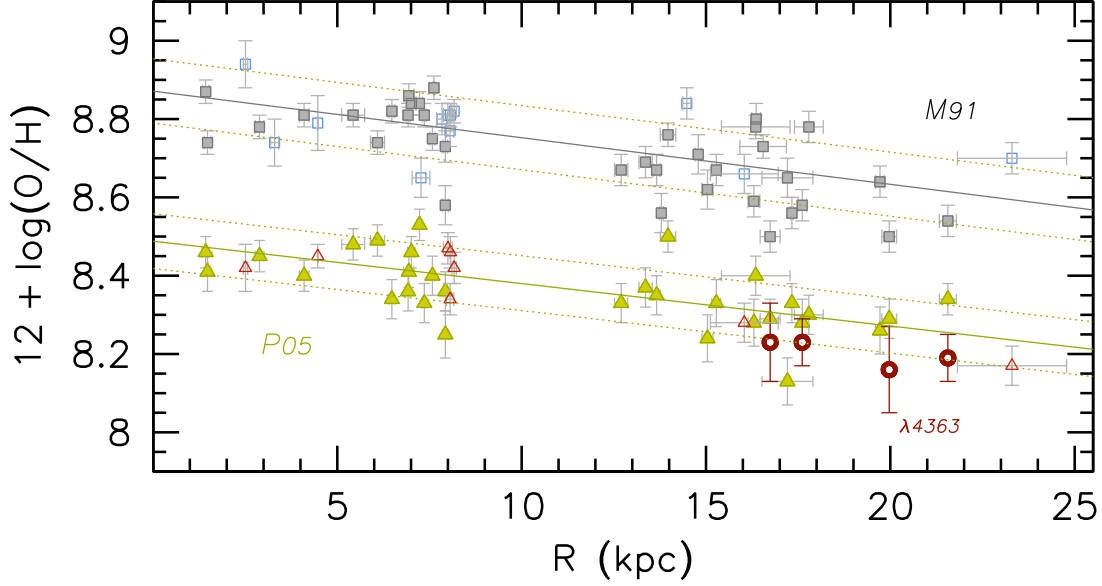


Figure 4. Galactocentric oxygen abundance gradient in NGC 4258. The abundances for the Gemini H II region sample calculated with the M91 and P05 calibrations are shown as full squares and full triangles, respectively. Open symbols (squares and triangles for M91 and P05, respectively) are used for the H II regions extracted from the literature. The corresponding regression lines, calculated accounting for errors in both coordinates, are shown by the grey and green lines. The open circles show the oxygen abundance of the four H II regions where the [O III] $\lambda 4363$ was detected. In several cases the errors in the deprojected galactocentric distances are smaller than the size of the symbols used.

With the oxygen abundances derived from the M91 calibration the regression to the data (grey line in Fig. 4) yields:

$$12 + \log(\text{O}/\text{H}) = 8.87 (\pm 0.02) - 0.012 (\pm 0.002) R_{\text{kpc}} \quad (1)$$

where R_{kpc} is the galactocentric distance measured in kpc. With the adopted values for the distance (7.2 Mpc) and the isophotal radius R_{25} (9/31), the gradient slope can also be expressed as $-0.23 \pm 0.04 \text{ dex } R_{25}^{-1}$ or $-0.025 \pm 0.004 \text{ dex arcmin}^{-1}$.

In the case of the abundances derived from the *P* method of P05 the linear fit is (green line in Fig. 4):

$$12 + \log(\text{O}/\text{H}) = 8.49 (\pm 0.02) - 0.011 (\pm 0.002) R_{\text{kpc}} \quad (2)$$

corresponding to $-0.21 \pm 0.03 \text{ dex } R_{25}^{-1}$ or $-0.023 \pm 0.003 \text{ dex arcmin}^{-1}$. The dotted lines in Fig. 4 show the 1σ scatter around these fits (0.08 and 0.07 dex, respectively).

It is worth pointing out the following:

- the slopes of the two fits agree within the uncertainties, but the intercepts differ by 0.38 dex. This is due to the aforementioned systematic offsets between different calibrations of strong-line indicators, in particular between one calibrated from photoionization models (M91) and one calibrated empirically (P05).

- a look at Fig. 4 suggests that in the inner 8 kpc the gradient is virtually flat, with constant $12 + \log(\text{O}/\text{H}) = 8.79 \pm 0.07$ (M91) and $12 + \log(\text{O}/\text{H}) = 8.40 \pm 0.07$ (P05), however this solution is not found to be statistically preferable over the single slope solution.

- the result on the abundance gradient *slope* appears to be relatively robust. We considered the R_{23} calibrations by

Zaritsky et al. (1994) and Tremonti et al. (2004), both of which are based on theoretical models, and obtained results that are in agreement with the two previous determinations, as Table 6 shows. It should also be noted that the Zaritsky et al. (1994) calibration yields the largest intercept value, 0.53 dex above the P05 calibration and 0.15 dex above the M91 calibration.

The data points corresponding to the [O III] $\lambda 4363$ -based abundances are shown as red circles (labeled $\lambda 4363$) in Fig. 4. Their positions in the plot are within $\sim 1 \sigma$ of the regression line for the abundances of the full sample based on the P05 method. This relatively good agreement is not surprising, since the *P* method was calibrated empirically from H II regions whose abundances were obtained from the use of the auroral lines. For Cepheid-related work it is worth pointing out that the abundances tied to the [O III] $\lambda 4363$ detections (i.e. those obtained from the P05 calibration) are to be considered in the T_e -based scale (Kennicutt et al. 2003, Sakai et al. 2004). Although the overall metallicity of NGC 4258 in the T_e scale might seem to be low, its characteristic oxygen abundance [$12 + \log(\text{O}/\text{H}) = 8.40$ at $R = 0.4 R_{25}$] is normal for this galaxy's luminosity and rotational velocity, according to the trends found by Pilyugin et al. (2004) using abundances of galaxies obtained from the *P* method, albeit with an O/H ratio slightly below average. We can also compare NGC 4258 to a galaxy with a well-determined, T_e -based abundance gradient like M101, which has an absolute luminosity $M_B = -20.9$, similar to that of NGC 4258 ($M_B = -20.8$). The slope of the abundance gradient in M101 is $-0.032 \text{ dex kpc}^{-1}$, with an extrapolated central abundance $12 + \log(\text{O}/\text{H}) = 8.75 \pm 0.05$ (Bresolin 2007). The ~ 0.26 dex lower intercept for NGC 4258 can be understood by recalling

Table 6
Results of linear regression to the abundance gradient

R_{23} calibration	Intercept	Slope		
(1)	(2)	dex kpc ⁻¹	dex R_{25} ⁻¹	dex arcmin ⁻¹
(1)	(2)	(3)	(4)	(5)
<i>This paper</i>				
McGaugh (1991)	8.87 ± 0.02	-0.012 ± 0.002	-0.23 ± 0.04	-0.025 ± 0.004
Pilyugin & Thuan (2005)	8.49 ± 0.02	-0.011 ± 0.002	-0.21 ± 0.03	-0.023 ± 0.003
Zaritsky et al. (1994)	9.02 ± 0.03	-0.013 ± 0.002	-0.25 ± 0.05	-0.027 ± 0.005
Tremonti et al. (2004)	8.94 ± 0.02	-0.011 ± 0.002	-0.22 ± 0.04	-0.023 ± 0.005
<i>Published</i>				
<i>Authors</i>				
Zaritsky et al. (1994)	9.17 ± 0.06	-0.029 ± 0.005	-0.58 ± 0.09	-0.062 ± 0.010
Dutil & Roy (1999)	8.86 ± 0.02	-0.012 ± 0.002	-0.23 ± 0.04	-0.025 ± 0.004
Pilyugin et al. (2004)	8.57	-0.010	-0.20	-0.021
Bono et al. (2008)	8.55	-0.010	-0.20	-0.021

that strongly barred galaxies³, in addition to shallower gradients, also display significantly lower (0.3-0.4 dex) central abundances compared to non-barred galaxies (Dutil & Roy 1999; see also Fig. 11 of Vila-Costas & Edmunds 1992).

As already pointed out, the absolute values of the chemical abundances are greatly dependent on the choice of abundance determination method. The P method by P05 provides results which are in good agreement with the auroral line-based abundances determined for a handful of objects. However, comparisons with independent methods would be highly desirable, in order to establish the absolute abundance scale in NGC 4258. This is relevant, for example, for the amount of the metallicity correction to the Cepheid-based distance modulus. Future spectroscopic studies of the stellar abundances in this galaxy are already planned by the author and his collaborators with observations at the Keck telescope. It is also interesting to note that the recent work by Konami et al. (2009) obtained a metallicity of the interstellar medium in NGC 4258 from observations with the Suzaku X-ray satellite. Their result, $\sim 0.5 Z_{\odot}$ in the Anders & Grevesse (1989) solar metallicity scale, corresponds approximately to $12 + \log(\text{O}/\text{H}) = 8.6$, i.e. an intermediate value between those indicated by the two methods used here.

5. PREVIOUS DETERMINATIONS OF THE ABUNDANCE GRADIENT

The oxygen abundance gradient of NGC 4258 was already derived as part of earlier spectroscopic studies of large samples of H II regions in different galaxies, in particular by Zaritsky et al. (1994, = ZKH), who also included spectrophotometric data obtained by Oey & Kennicutt (1993), for a total number of about 15 objects. However, before a direct comparison with our results can be made it is necessary to homogenize the distances and diameters adopted by the different authors. In particular, ZKH adopted an isophotal radius of 7.92 from the RC2 (de Vaucouleurs et al. 1976), which differs significantly from the value of 9.31 that we adopted from the RC3 (de Vaucouleurs et al. 1991). Thus, the gradient published by ZKH:

$$12 + \log(\text{O}/\text{H}) = 8.97 (\pm 0.06) - 0.49 (\pm 0.08) (R/R_{25} - 0.4)$$

³ Evidence for the presence of a bar in NGC 4258 has been provided by van Albada (1980).

becomes, after renormalization:

$$12 + \log(\text{O}/\text{H}) = 9.166 (\pm 0.06) - 0.029 (\pm 0.005) R_{\text{kpc}}$$

This is a significantly steeper gradient than the one we have derived earlier in Eq. (1) and (2). It appears that the ZKH result is highly dependent on the abundance calculated for one of the two outermost H II regions, number 8 in their list (our number 30, for which we also obtained a [O III] $\lambda 4363$ detection). The problem is not in the line fluxes, since we measure very similar [O II] $\lambda 3727$ and [O III] $\lambda \lambda 4959, 5007$ line intensities. However, the application of ZKH's own calibration of R_{23} provides quite a low oxygen abundance for this particular H II region, $12 + \log(\text{O}/\text{H}) = 8.41$, about 0.4 dex lower than other objects at a similar galactocentric distance. This anomaly appears to be related to the high R_{23} value. In fact, two additional H II regions in our sample (24 and 36), which also have $\log(R_{23}) > 0.9$, display peculiarly low O/H abundances when adopting the ZKH and the Tremonti et al. (2004) R_{23} calibrations. This suggests a systematic problem with the functional form of these calibrations at high R_{23} values. Therefore, we have excluded these three H II regions to calculate the regressions whose parameters are shown in Table 6.

As part of an abundance study of eight early-type spiral galaxies, Dutil & Roy (1999) measured the abundance gradient of NGC 4258, using a spectrophotometric technique based on narrow-band imaging through filters centered on important nebular emission lines and applied to 122 H II regions. They adopted as their abundance indicator the [O III] $\lambda 5007$ /[N II] $\lambda 6583$ line ratio, calibrated as a function of O/H by Edmunds & Pagel (1984). These authors adopted a distance to NGC 4258 of 7.3 Mpc, i.e. virtually the same one used here. They obtained the following oxygen abundance gradient:

$$12 + \log(\text{O}/\text{H}) = 8.86 (\pm 0.02) - 0.012 (\pm 0.002) R_{\text{kpc}}$$

which is the same we derive from our sample using the M91 R_{23} calibration. Dutil & Roy (1999) do not provide a list of line fluxes for their targets, so that we cannot compare their measurements with ours on an object-by-object basis. However, the excellent agreement between the two gradient determinations indicates that the imaging spectrophotometry of Dutil & Roy (1999) is not affected by important systematic

uncertainties, which could originate especially from the subtraction of the stellar underlying continuum, and which could introduce biases in the chemical abundances derived with this technique (Dutil & Roy 2001).

More recently, Bono et al. (2008) reconsidered the abundance gradient in NGC 4258 in their reanalysis of the Cepheid variables discovered by Macri et al. (2006). Bono et al. (2008) found that the comparison of the data with pulsation models suggested both a lower metallicity and a shallower abundance gradient in NGC 4258 than one obtains from the ZKH paper. Taking the few data points published by Díaz et al. (2000), these authors derived an abundance gradient which, after renormalization to the quantities adopted in our paper, has a slope of $-0.010 \text{ dex kpc}^{-1}$, with a central abundance $12 + \log(\text{O}/\text{H}) = 8.55$. This agrees also with the study by Pilyugin et al. (2004), who used the P parameter method to measure abundance gradients from data in the literature for more than 50 galaxies. Finally, Riess et al. (2009a) obtained abundances from Keck observations. They do not provide information about their targets and their derived abundances, but from their Table 12 we infer a slope of $-0.017 \text{ dex kpc}^{-1}$. This gradient is possibly too steep because of the presence of two H II regions at large galactocentric distance and low O/H ratio (as judged from their Fig. 11), which might suffer from the same large- R_{23} issue mentioned earlier.

To summarize, the evidence from most of the results published in the literature and from the analysis of the new Gemini data presented here is that the abundance gradient in NGC 4258 is very shallow, with a slope of approximately $-0.012 \text{ dex kpc}^{-1}$, in contrast with the steeper (by a factor of 2.5) slope obtained by ZKH. This shallow abundance gradient is not surprising, in view of the fact that barred galaxies (like NGC 4258) and spiral galaxies of early type have smaller slopes compared to non-barred and late-type galaxies (e.g. Vila-Costas & Edmunds 1992, Zaritsky et al. 1994). For example, Vila-Costas & Edmunds (1992) found that the barred galaxies in their sample have slopes that are shallower than $-0.05 \text{ dex kpc}^{-1}$, while non-barred galaxies can have slopes up to four times steeper. This behavior is also predicted by numerical simulations of barred galaxies (Friedli et al. 1994).

6. THE METALLICITY DEPENDENCE OF THE CEPHEID PERIOD-LUMINOSITY RELATION IN NGC 4258

Macri et al. (2006) have identified 281 Cepheid variables in two *HST* ACS fields of NGC 4258, whose centers are located $179''$ (6.25 kpc, ‘inner’ field) and $490''$ (17.11 kpc, ‘outer’ field) from the galaxy nucleus (deprojected distances). Our spectroscopic coverage of H II regions in NGC 4258 was designed to allow the measurement of nebular abundances at the same galactocentric distances of the Cepheids, as visualized in Fig. 5. The extinction-corrected distance moduli of the two fields relative to the LMC, as determined by Macri et al. (2006) from the *BVI* P - L relations of a restricted sample of Cepheids, are $\Delta\mu_o = 10.87$ (inner field) and $\Delta\mu_o = 10.71$. These authors ascribed this result to the difference in metallicity between the two fields, as a consequence of the dependence of the P - L relation on metal content. Adopting the radial abundance gradient measured by ZKH, they fitted the distribution of the distance moduli derived for individual Cepheids as a function of the O/H ratio, to obtain a value of the parameter $\gamma = \delta\mu_o / \delta\log Z = -0.29 \pm 0.09$ (random) \pm

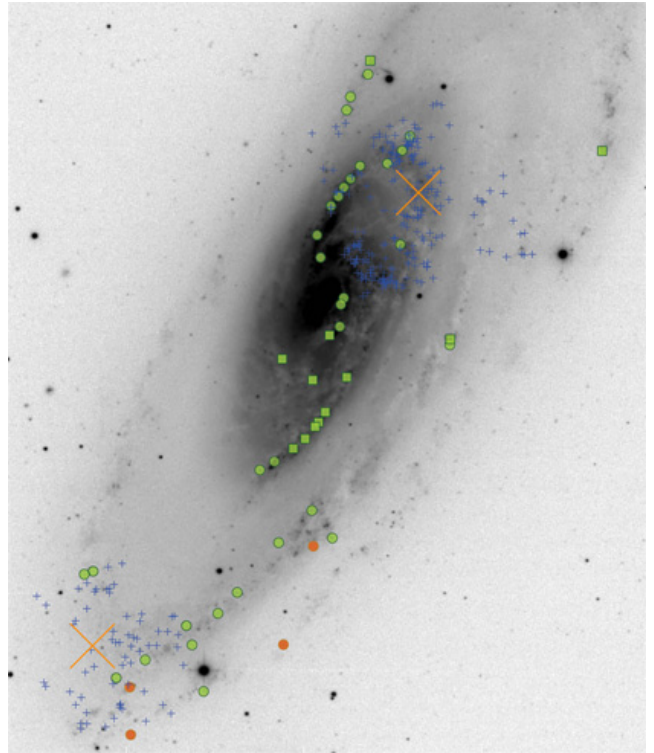


Figure 5. The distribution of Cepheids in NGC 4258 (Macri et al. 2006, blue crosses) compared with the location of the H II regions studied in this work (circles for the new Gemini sample, squares for the objects drawn from the literature). The red circles represent the H II regions with the [O III] $\lambda 4363$ detections. The big crosses show the centers of the two ACS fields observed by Macri et al. (2006). *B*-band image courtesy of L. van Zee.

0.05 (systematic) mag dex^{-1} . This γ value is in good agreement with other empirical determinations (see a review of the extensive data present in the literature by Romaniello et al. 2008). Here, we just mention some of the recent results based on the differential analysis of Cepheids located at different distances from the center of their host galaxy. Kennicutt et al. (1998) determined a value of $\gamma = -0.24 \pm 0.16 \text{ mag dex}^{-1}$ from *HST* observations of two fields in M101. More recently, Scowcroft et al. (2009) performed a similar experiment in the galaxy M33, obtaining $\gamma = -0.29 \pm 0.11 \text{ mag dex}^{-1}$. It is well-known that these empirical results, showing that metal-rich Cepheids are brighter than metal-poor ones, are at variance with the predictions from pulsation models, i.e. that Cepheids become *fainter* with increasing metallicity, with a dependence on the passbands of the observations (Fiorentino et al. 2007). The latter finding is backed by recent investigations of the iron content of Galactic and Magellanic Cloud Cepheids (Romaniello et al. 2008).⁴

For the case of NGC 4258, as demonstrated in Sect. 4 and 5, the ZKH abundance gradient adopted by Macri et al. (2006) is much steeper than our new observations and other data in the literature indicate. Instead of a difference in oxygen abundance of $\delta\log(\text{O}/\text{H}) = 0.31 \text{ dex}$ between the inner and outer fields, as one would derive from the ZKH gradient, we measure $\delta\log(\text{O}/\text{H}) \simeq 0.13 \text{ dex}$. Correspondingly the metallicity correction factor would become $\gamma = -0.69 \text{ mag dex}^{-1}$, an un-

⁴ The γ values reported here refer to distances measured from *VI* photometry. The metallicity effect is predicted to vary with the use of different passbands.

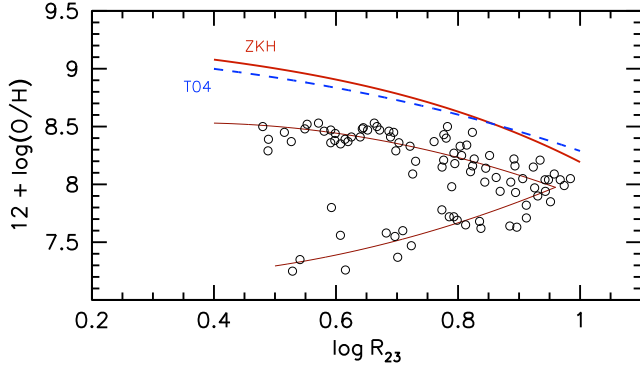


Figure 6. $\log(R_{23})$ vs. $12 + \log(\text{O}/\text{H})$ for the same sample of extragalactic H II regions shown in Fig. 3. The curves in the upper part represent the R_{23} calibrations by Zaritsky et al. (1994, continuous line, ZKH) and Tremonti et al. (2004, dashed line, T04).

acceptably large value from both the empirical and theoretical standpoints. We are drawn to conclude, together with Bono et al. (2008), that, because of its shallow gradient, NGC 4258 (like any other barred galaxy) is not the ideal laboratory to perform differential studies of the metallicity dependence of the Cepheid pulsation properties.

What is then the origin of the observed distance modulus difference between the inner and outer fields in NGC 4258? While we cannot presently discard the effects of varying Cepheid helium abundance or differences in the reddening law (Mager et al. 2008), the presence of systematic errors affecting the Cepheid distance of the outer field appears as a possible solution (di Benedetto 2008). In particular, Mager et al. (2008) showed how the outer field Cepheids, contrary to the inner field ones, do not evenly populate the instability strip, projected into the P - L relation. Instead, their magnitudes are skewed towards faint levels, thus artificially increasing the distance modulus.

6.1. The metallicity of NGC 4258 on the T_e scale

The detection of the $[\text{O III}] \lambda 4363$ line and the derivation of O/H ratios from the strength of this line in four of the outer H II regions has allowed us to place the chemical abundance of NGC 4258 on the T_e scale on rather solid evidence, in combination with the use of the P05 calibration of the R_{23} metallicity indicator for the innermost part of the galaxy. From Eq. 2 we obtain:

$$\text{inner field: } 12 + \log(\text{O}/\text{H}) = 8.42 \pm 0.03$$

$$\text{outer field: } 12 + \log(\text{O}/\text{H}) = 8.30 \pm 0.06$$

If for the outer field we take the $\lambda 4363$ -based abundance for objects 24 and 34 (their galactocentric distance matches that of the center of the outer ACS field) we obtain $12 + \log(\text{O}/\text{H}) = 8.23 \pm 0.09$. Given the size of the errors, and the statistical nature of the R_{23} indicator, we do not regard this small difference as a significant discrepancy, and adopt the former result for consistency with the inner field abundance, which can only be derived from the linear regression.

It is interesting to compare these abundances with those proposed by other authors working on the Cepheid distance scale. Sakai et al. (2004) obtained a transformation between nebular oxygen abundances of Cepheid host galaxies based on the ZKH abundance scale, and those one derives using the auroral line method, which is based on the ability to directly

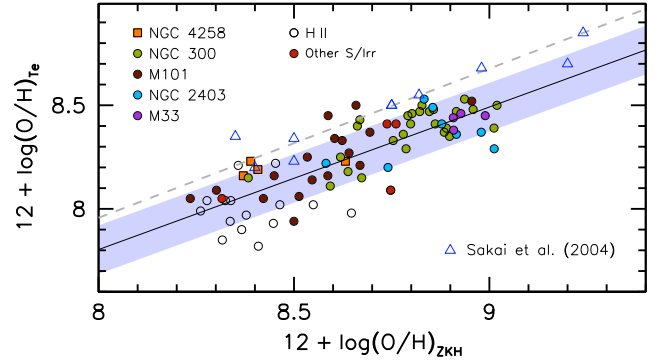


Figure 7. Comparison between the oxygen abundances in the ZKH and T_e (i.e. $[\text{O III}] \lambda 4363$ -based) scales. The sample of H II regions is the same as in Fig. 3. The linear regression to the H II region sample is shown by the straight line, and the $\pm 1\sigma$ scatter is represented by the shaded area. The high-metallicity (R_{23} upper branch) galaxy data points of Sakai et al. (2004) are shown by the blue triangles. The dashed line is the linear fit to the latter by Saha et al. (2006).

measure the electron temperature of the ionized gas (hence the ‘ T_e -based’ definition). As already stressed, the T_e abundances are systematically lower than those derived from the ZKH and most of the other strong-line metallicity indicators (Kennicutt et al. 2003; Bresolin et al. 2004). The effect is stronger at high metallicity, thus compressing the metallicity range spanned by star-forming galaxies. This can be appreciated in Fig. 6, where the same data points of Fig. 3 are shown, together with the curves corresponding to the ZKH (continuous line) and Tremonti et al. (2004, dashed line) R_{23} calibrations. These two curves are seen to be diverging from the T_e -based abundances, shown by the dots, as the metallicity increases, with the effect being stronger in this example for the ZKH calibration.

It should also be recalled that most of the nebular work of the past few years has adopted the recent solar oxygen abundance derived from 3-D hydrodynamical models of the Sun, which yield $12 + \log(\text{O}/\text{H})_{\odot} = 8.69$ (Allende Prieto et al. 2001; Asplund et al. 2009), 0.24 dex below the Anders & Grevesse (1989) value. In this scale, for example, the LMC is found to have a nebular oxygen abundance of $12 + \log(\text{O}/\text{H})_{\text{LMC}} = 8.36 \pm 0.10$. This value is the mean obtained by the author (see Appendix) from a reanalysis of published emission line fluxes carried out with consistent atomic data. This is in excellent agreement with results from other stellar indicators, for example Cepheids, for which Romaniello et al. (2008) found $[\text{Fe}/\text{H}]_{\text{LMC}} = -0.33 \pm 0.13$, corresponding to $12 + \log(\text{O}/\text{H}) = 8.36 \pm 0.13$.

Saha et al. (2006) and Bono et al. (2010) performed polynomial fits to the Sakai et al. (2004) data points, producing a relation between O/H abundance ratios in the ZKH system and the T_e system. Using the data in Table 7 of Bono et al. (2010) we find that in the case of NGC 4258 the transformed $12 + \log(\text{O}/\text{H})$ abundances are 0.2 dex larger than the abundances that we measure: 8.64 vs. 8.42 for the inner field, 8.50 vs. 8.30 for the outer field. To investigate the origin of this discrepancy, the relation between the oxygen abundances in the ZKH and T_e scales for the same sample of H II regions shown in Fig. 3 was considered. The result is illustrated in Fig. 7, where the abundances from Table 4 of Sakai et al. (2004, open triangles) and the linear fit to the latter by Saha et al. (2006, dashed line) are included. Only points in the R_{23} upper branch are shown, because the ZKH calibration only applies to

that regime (the transformation between the two abundance scales below $12 + \log(\text{O}/\text{H})_{\text{ZKH}} \simeq 8.2$ is thus undefined). The linear fit to the individual H II region data (continuous line) in Fig. 7 lies 0.15 dex below the Saha et al. (2006) regression at $x = 12 + \log(\text{O}/\text{H})_{\text{ZKH}} = 8.5$. The new transformation is:

$$12 + \log(\text{O}/\text{H})_{T_e} = 0.69 (\pm 0.06) x + 2.30 (\pm 0.51). \quad (3)$$

Only two data points from Sakai et al. (2004), the inner and outer fields of M101, fall within the 1σ scatter (± 0.11 dex) of this regression. The origin of the T_e -based abundances provided by Sakai et al. (2004, Table 4) is not specified in their paper, so it is difficult to ascertain the reason for the discrepancy for the remaining upper branch metallicities. It should also be added that at the time of their publication the systematic offset between strong-line abundances and direct abundances in H II regions had just become clear (Kennicutt et al. 2003), and that since then the number of high-metallicity H II regions with auroral line detections has increased significantly (e.g. Bresolin et al. 2009).

The comparison between our new and the previous ZKH- T_e abundance transformations explains the reason why the metallicities we derive for the two fields in NGC 4258 are smaller than those obtained from the Saha et al. (2006) or Bono et al. (2010) transformations. It also indicates that the latter should be revisited according to Eq. 3 if one wishes to transform in a consistent way the strong-line abundances in the ZKH scale to the T_e scale. This is done in the Appendix for a number of Cepheid host galaxies.

We would also like to point out that the fact that the multiplicative coefficient for x in Eq. 3 differs significantly from unity (the same information is conveyed by the divergence of the ZKH curve in Fig. 6 from the T_e -based empirical abundances with increasing metallicity) implies that abundance gradient slopes can depend on the choice of abundance determination methods. The effect is small in the case of NGC 4258, where the gradient slope is very shallow and the metallicity range over the full extent of the galactic disk is ~ 0.2 dex. However, for galaxies with steeper abundance gradients the effect could become significant.

6.2. Consequences for the Cepheid distances

The abundances in the T_e scale place the inner field of NGC 4258 essentially at the metallicity of the LMC, rather than at the Galactic value ($12 + \log(\text{O}/\text{H}) \simeq 8.7$), which has been usually adopted in the literature to estimate the distance modulus to NGC 4258 (e.g. Benedict et al. 2007). How would this affect the Cepheid distance to NGC 4258 from the Macri et al. (2006) data? To answer this question, two methods have been considered:

a) we take the extinction-corrected distance modulus of the inner field of NGC 4258 relative to the LMC from Macri et al. (2006), $\Delta\mu_o = 10.71 \pm 0.04_r \pm 0.05_s$, and apply no metallicity correction, since the O/H abundance is the same. Thus, adopting $\mu_{\text{LMC}} = 18.5$ from the *HST* Key Project (Freedman et al. 2001), we obtain $\mu_{\text{NGC 4258}} = 29.21 \pm 0.04_r \pm 0.05_s$. Alternatively, if we assume the maser distance modulus to NGC 4258, $29.29 \pm 0.09_r \pm 0.12_s$ we would obtain $\mu_{\text{LMC}} = 18.58 \pm 0.10_r \pm 0.13_s$.

b) we follow Mager et al. (2008), who restricted the Macri et al. (2006) sample to Cepheids with periods above 10

days, for consistency with the procedure adopted by the Key Project. For the inner field they obtain $\mu_0 = 29.26 \pm 0.03$. The metallicity correction applied by the Key Project is $\delta\mu_z = -0.2[(\text{O}/\text{H}) - (\text{O}/\text{H})_{\text{LMC}}] \text{ mag dex}^{-1}$. Since we are testing the idea that the inner field has the same metallicity of the LMC, this correction would be zero in our case. Thus, $\mu_{0,\text{NGC 4248}} = 29.26 \pm 0.03$.

We also note that the adoption of an LMC-like metallicity for the inner field explains the finding by Tammann et al. (2008) that the *BVI* *P-L* relations in this field agree with those in the LMC, rather than those for the higher Galactic metallicity, without the need to invoke the existence of a second parameter, such as the helium abundance. In virtue of the shallow abundance gradient, the outer field is also at a similar metallicity. We can also conclude that the adoption of the T_e abundance scale for NGC 4258, as presented here, would yield results that are compatible with the Key Project and with the geometric distance from the water masers.

6.3. Reliability of the absolute T_e abundances

Although our analysis of H II region data can be used to place the metallicity of the interstellar medium of NGC 4258 on the T_e scale, there are some important considerations that need to be taken into account when dealing with nebular abundances obtained from the [O III] $\lambda 4363$ auroral line. First is the effect of dust depletion onto dust grains. Recent estimates of the oxygen depletion factor obtained from the study of the Orion nebula are in the range between 0.08 dex (Esteban et al. 2004) and 0.12 dex (Mesa-Delgado et al. 2009). Secondly, accounting for the presence of temperature fluctuations in the ionized gas has the effect of increasing the metal abundances (Peimbert 1967), yielding results that are compatible with those from metal recombination lines. For these reasons, the T_e -based abundances are often regarded as lower limits to the real abundances.

In the case of the Orion nebula, whose T_e -based oxygen abundance is $12 + \log(\text{O}/\text{H}) = 8.51 \pm 0.03$ (Esteban et al. 2004), the sum of these two effects is about 0.25 dex. Recently Simón-Díaz & Stasińska (2010) have shown that the oxygen abundance for the gas phase (from metal recombination lines) in the Orion nebula, increased by the amount locked in dust grains, is consistent with the value of $12 + \log(\text{O}/\text{H}) = 8.74 \pm 0.04$ derived from 13 B stars in the Ori OB1 association. This compares very well with the Galactic neighborhood value of $12 + \log(\text{O}/\text{H}) = 8.76 \pm 0.03$, calculated by Przybilla et al. (2008) from B stars. These results suggest that the T_e -based results could systematically underestimate the oxygen abundance by 0.25 dex.

On the other hand, the addition of the depletion correction factor to the recombination line abundance of 30 Dor in the LMC gives an abundance, $12 + \log(\text{O}/\text{H}) = 8.61 \pm 0.03$ (Peimbert & Peimbert 2010), which is clearly at variance with respect to the B-star [$12 + \log(\text{O}/\text{H}) = 8.33 \pm 0.08$, Hunter et al. 2007] and Cepheid (Romaniello et al. 2008) metallicities, unless it is assumed that the present-day chemical composition of the LMC is highly non-uniform. Therefore, in this case the T_e -based oxygen abundance is in excellent agreement with the stellar one, as is also found for the SMC (e.g. Trundle & Lennon 2005), where $12 + \log(\text{O}/\text{H}) = 8.03 \pm 0.09$ (see Appendix).

6.4. The case of M33

We also briefly consider the case of M33, where Scowcroft et al. (2009) have determined $\gamma = -0.29 \pm 0.11 \text{ mag dex}^{-1}$ from the difference in distance modulus between an inner and an outer field, and adopting a metallicity gradient obtained from H II regions which is very steep ($-0.19 \text{ dex kpc}^{-1}$) in the central 3 kpc, and rather shallow ($-0.038 \text{ dex kpc}^{-1}$) beyond this radius (taken from Magrini et al. 2007). The choice of this bimodal abundance gradient is questionable, and the most recent works on the chemical composition of the ionized gas (Crockett et al. 2006; Rosolowsky & Simon 2008; Bresolin et al. 2010) and young supergiants (U et al. 2009) in M33 yield a single-slope gradient, with a shallow value throughout the disk of the galaxy. The most recent and arguably one of the most accurate determinations to date of the H II region radial oxygen abundance gradient in M33 has been obtained by Bresolin et al. (2010), who measured a slope of $-0.030 \pm 0.008 \text{ dex kpc}^{-1}$ from [O III] $\lambda 4363$ detections, which extend into the inner kpc of the galaxy. They found no indication of an upward turn in the nebular abundances in the inner 3 kpc, where they measured $12 + \log(\text{O}/\text{H}) \simeq 8.4$, instead of $12 + \log(\text{O}/\text{H}) = 8.85$, as used by Scowcroft et al. (2009). The adoption of such a shallow abundance slope yields a total range in O/H between the inner and outer regions of M33 of only 0.14 dex. This, combined with the distance moduli obtained at the two different galactocentric distances by Scowcroft et al. (2009), would result in an exceedingly strong metallicity effect on the Cepheid-derived distances, with $\gamma \simeq -1.2 \text{ mag dex}^{-1}$.

We note that a bias from small number statistics, similar to the one encountered in NGC 4258, could also be affecting the M33 result by Scowcroft et al. (2009). As can be seen from the P - L and Period-Wesenheit relations shown in their Fig. 5 and 6, the scatter for the outer field Cepheids at constant period is much smaller than that for the inner field, indicating that the width of the instability strip is not sufficiently sampled. This effect is exacerbated by the scarcity of Cepheids with periods ≥ 10 days in their outer field (only two are found). We reach the same conclusion we drew for NGC 4258, that γ cannot be reliably derived in M33 with present Cepheid samples. A more reliable approach to constrain the metallicity effect on Cepheid-based extragalactic distances is represented by the comparison with the distances provided by the TRGB method as a function of the host galaxy metallicity (Sakai et al. 2004; Tammann et al. 2008; Bono et al. 2010), provided the latter is measured consistently, for example in the T_e scale, as explained in § 6.1.

7. SUMMARY

This paper combined new deep spectroscopic observations of 36 H II regions in NGC 4258 obtained with the Gemini telescope with data from the literature, to measure the oxygen abundance gradient for this galaxy. Strong-line abundances have been derived from two different calibrations of the R_{23} indicator, the one by McGaugh (1991) and the one by Pilyugin & Thuan (2005). For four of the outermost H II regions the [O III] $\lambda 4363$ auroral line has been detected, and used to measure the nebular abundances directly in the T_e scale. The main results are summarized here:

1. The radial abundance gradient in NGC 4258 has a slope of approximately $-0.012 \text{ dex kpc}^{-1}$, which is a factor of 2.5 shallower than the value reported by Zaritsky et al. (1994) and

adopted by Macri et al. (2006) to infer a metallicity correction of Cepheid distances of $\gamma = -0.29 \text{ mag dex}^{-1}$.

2. Adopting the shallow gradient resulting from the new analysis would yield an unrealistically large metallicity correction for the Cepheid distances. This indicates that NGC 4258, with its present sets of Cepheid observations, is not suited for a differential metallicity study to measure γ reliably.

3. The [O III] $\lambda 4363$ detections and the P05 R_{23} calibration provide the oxygen abundances in the T_e scale. In this scale, the inner field of NGC 4258 has an LMC-like O/H ratio, and not a Galactic one.

4. The same systematic biases from small number statistics that might explain the difference in distance moduli between the inner and outer regions of NGC 4258 (Mager et al. 2008) seem to affect also the differential analysis of M33 Cepheids by Scowcroft et al. (2009).

5. The transformation between ‘old’ H II region metallicities in the Zaritsky et al. (1994) system and the T_e system by Sakai et al. (2004) is affected by a systematic error of about 0.2 dex. Using recent observations of H II regions with auroral line-based abundances, a revised transformation has been calculated.

The main results of this work can be tested in the near future, with the availability of larger samples of Cepheids in the outer regions of NGC 4258 and M33, to remove potential statistical biases, and with the derivation of blue supergiant metallicities, which will help to establish the absolute scale of the chemical abundances in NGC 4258.

FB gratefully acknowledges the support from the National Science Foundation grants AST-0707911 and AST-1008798, and thanks R.P. Kudritzki for discussions and comments on an earlier draft of this paper. The Gemini observations used in this paper were obtained under program GN-2010A-Q-25.

Facility: Gemini:Gillett (GMOS)

REFERENCES

- Allende Prieto, C., Lambert, D. L., & Asplund, M. 2001, *ApJ*, 556, L63
 An, D., Terndrup, D. M., & Pinsonneault, M. H. 2007, *ApJ*, 671, 1640
 Anders, E., & Grevesse, N. 1989, *Geochim. Cosmochim. Acta*, 53, 197
 Asplund, M., Grevesse, N., Sauval, A. J., & Scott, P. 2009, *ARA&A*, 47, 481
 Benedict, G. F., et al. 2007, *AJ*, 133, 1810
 Bono, G., Caputo, F., Fiorentino, G., Marconi, M., & Musella, I. 2008, *ApJ*, 684, 102
 Bono, G., Caputo, F., Marconi, M., & Musella, I. 2010, *ApJ*, 715, 277
 Bresolin, F. 2007, *ApJ*, 656, 186
 Bresolin, F. 2008, in *The Metal-Rich Universe*, ed. G. Israelian & G. Meynet, 155
 Bresolin, F., Garnett, D. R., & Kennicutt, R. C. 2004, *ApJ*, 615, 228
 Bresolin, F., Gieren, W., Kudritzki, R., Pietrzyński, G., Urbaneja, M. A., & Carraro, G. 2009, *ApJ*, 700, 309
 Bresolin, F., Kennicutt, Jr., R. C., & Garnett, D. R. 1999, *ApJ*, 510, 104
 Bresolin, F., Pietrzyński, G., Urbaneja, M. A., Gieren, W., Kudritzki, R.-P., & Venn, K. A. 2006, *ApJ*, 648, 1007
 Bresolin, F., Schaerer, D., González Delgado, R. M., & Stasińska, G. 2005, *A&A*, 441, 981
 Bresolin, F., Stasińska, G., Vílchez, J. M., Simon, J. D., & Rosolowsky, E. 2010, *MNRAS*, 404, 1679
 Bresolin, F., Urbaneja, M. A., Gieren, W., Pietrzyński, G., & Kudritzki, R.-P. 2007, *ApJ*, 671, 2028

- Courtes, G., Petit, H., Hua, C. T., Martin, P., Blecha, A., Huguenin, D., & Golay, M. 1993, *A&A*, 268, 419
- Crockett, N. R., Garnett, D. R., Massey, P., & Jacoby, G. 2006, *ApJ*, 637, 741
- de Vaucouleurs, G., de Vaucouleurs, A., Corwin, Jr., H. G., Buta, R. J., Paturel, G., & Fouque, P. 1991, *Third reference catalogue of bright galaxies* (Springer-Verlag Berlin Heidelberg New York)
- de Vaucouleurs, G., de Vaucouleurs, A., & Corwin, J. R. 1976, *Second reference catalogue of bright galaxies* (University of Texas Press)
- di Benedetto, G. P. 2008, *MNRAS*, 390, 1762
- Díaz, A. I., Castellanos, M., Terlevich, E., & Luisa García-Vargas, M. 2000, *MNRAS*, 318, 462
- Dufour, R. J. 1975, *ApJ*, 195, 315
- Dufour, R. J., & Harlow, W. V. 1977, *ApJ*, 216, 706
- Dufour, R. J., Shields, G. A., & Talbot, Jr., R. J. 1982, *ApJ*, 252, 461
- Dutil, Y., & Roy, J.-R. 1999, *ApJ*, 516, 62
- . 2001, *AJ*, 122, 1644
- Edmunds, M. G., & Pagel, B. E. J. 1984, *MNRAS*, 211, 507
- Esteban, C., Bresolin, F., Peimbert, M., García-Rojas, J., Peimbert, A., & Mesa-Delgado, A. 2009, *ApJ*, 700, 654
- Esteban, C., Peimbert, M., García-Rojas, J., Ruiz, M. T., Peimbert, A., & Rodríguez, M. 2004, *MNRAS*, 355, 229
- Ferrarese, L., et al. 2000, *ApJS*, 128, 431
- Fiorentino, G., Marconi, M., Musella, I., & Caputo, F. 2007, *A&A*, 476, 863
- Freedman, W. L., & Madore, B. F. 2010, *ARA&A*, 48, 673
- Freedman, W. L., et al. 1994, *ApJ*, 427, 628
- . 2001, *ApJ*, 553, 47
- Friedli, D., Benz, W., & Kennicutt, R. 1994, *ApJ*, 430, L105
- García-Rojas, J., Esteban, C., Peimbert, A., Rodríguez, M., Peimbert, M., & Ruiz, M. T. 2007, *Revista Mexicana de Astronomía y Astrofísica*, 43, 3
- Garnett, D. R., Shields, G. A., Skillman, E. D., Sagan, S. P., & Dufour, R. J. 1997, *ApJ*, 489, 63
- Guseva, N. G., Papaderos, P., Meyer, H. T., Izotov, Y. I., & Fricke, K. J. 2009, *A&A*, 505, 63
- Herrnstein, J. R., Moran, J. M., Greenhill, L. J., & Trotter, A. S. 2005, *ApJ*, 629, 719
- Herrnstein, J. R., et al. 1999, *Nature*, 400, 539
- Hook, I. M., Jørgensen, I., Allington-Smith, J. R., Davies, R. L., Metcalfe, N., Murowinski, R. G., & Crampton, D. 2004, *PASP*, 116, 425
- Humphreys, E. M. L., Reid, M. J., Greenhill, L. J., Moran, J. M., & Argon, A. L. 2008, *ApJ*, 672, 800
- Hunter, I., et al. 2007, *A&A*, 466, 277
- Izotov, Y. I., Thuan, T. X., & Lipovetsky, V. A. 1994, *ApJ*, 435, 647
- Kennicutt, R. C., Bresolin, F., & Garnett, D. R. 2003, *ApJ*, 591, 801
- Kennicutt, Jr., R. C., Stetson, P. B., Saha, A., et al. 1998, *ApJ*, 498, 181
- Kewley, L. J., & Ellison, S. L. 2008, *ApJ*, 681, 1183
- Kniazev, A. Y., Grebel, E. K., Pustilnik, S. A., Pramskij, A. G., & Zucker, D. B. 2005, *AJ*, 130, 1558
- Kobulnicky, H. A., Skillman, E. D., Roy, J., Walsh, J. R., & Rosa, M. R. 1997, *ApJ*, 477, 679
- Konami, S., et al. 2009, *PASJ*, 61, 941
- Kudritzki, R.-P., Urbaneja, M. A., Bresolin, F., Przybilla, N., Gieren, W., & Pietrzyński, G. 2008, *ApJ*, 681, 269
- Kuzio de Naray, R., McGaugh, S. S., & de Blok, W. J. G. 2004, *MNRAS*, 355, 887
- Lee, H., Skillman, E. D., & Venn, K. A. 2005, *ApJ*, 620, 223
- . 2006, *ApJ*, 642, 813
- Leonard, D. C., Kanbur, S. M., Ngeow, C. C., & Tanvir, N. R. 2003, *ApJ*, 594, 247
- López-Sánchez, Á. R., Esteban, C., García-Rojas, J., Peimbert, M., & Rodríguez, M. 2007, *ApJ*, 656, 168
- Macri, L. M., Stanek, K. Z., Bersier, D., Greenhill, L. J., & Reid, M. J. 2006, *ApJ*, 652, 1133
- Mager, V. A., Madore, B. F., & Freedman, W. L. 2008, *ApJ*, 689, 721
- Magrini, L., Vílchez, J. M., Mampaso, A., Corradi, R. L. M., & Leisy, P. 2007, *A&A*, 470, 865
- McCommas, L. P., Yoachim, P., Williams, B. F., Dalcanton, J. J., Davis, M. R., & Dolphin, A. E. 2009, *AJ*, 137, 4707
- McGaugh, S. S. 1991, *ApJ*, 380, 140
- Menzel, D. H., Aller, L. H., & Hebb, M. H. 1941, *ApJ*, 93, 230
- Mesa-Delgado, A., Esteban, C., García-Rojas, J., Luridiana, V., Bautista, M., Rodríguez, M., López-Martín, L., & Peimbert, M. 2009, *MNRAS*, 395, 855
- Newman, J. A., Ferrarese, L., Stetson, P. B., Maoz, E., Zepf, S. E., Davis, M., Freedman, W. L., & Madore, B. F. 2001, *ApJ*, 553, 562
- Oey, M. S., & Kennicutt, Jr., R. C. 1993, *ApJ*, 411, 137
- Pagel, B. E. J., Edmunds, M. G., Blackwell, D. E., Chun, M. S., & Smith, G. 1979, *MNRAS*, 189, 95
- Pagel, B. E. J., Edmunds, M. G., Fosbury, R. A. E., & Webster, B. L. 1978, *MNRAS*, 184, 569
- Peña, M., Stasińska, G., & Richer, M. G. 2007, *A&A*, 476, 745
- Peimbert, A., & Peimbert, M. 2010, *ApJ*, 724, 791
- Peimbert, M. 1967, *ApJ*, 150, 825
- Pettini, M., & Pagel, B. E. J. 2004, *MNRAS*, 348, L59
- Pilyugin, L. S., & Thuan, T. X. 2005, *ApJ*, 631, 231
- Pilyugin, L. S., Vílchez, J. M., & Contini, T. 2004, *A&A*, 425, 849
- Przybilla, N., Nieva, M.-F., & Butler, K. 2008, *ApJ*, 688, L103
- Riess, A. G., Li, W., Stetson, P. B., Filippenko, A. V., Jha, S., Kirshner, R. P., Challis, P. M., Garnavich, P. M., & Chornock, R. 2005, *ApJ*, 627, 579
- Riess, A. G., et al. 2009b, *ApJ*, 699, 539
- . 2009a, *ApJS*, 183, 109
- Romaniello, M., et al. 2008, *A&A*, 488, 731
- Rosolowsky, E., & Simon, J. D. 2008, *ApJ*, 675, 1213
- Russell, S. C., & Dopita, M. A. 1990, *ApJS*, 74, 93
- Saha, A., Thim, F., Tammann, G. A., Reindl, B., & Sandage, A. 2006, *ApJS*, 165, 108
- Sakai, S., Ferrarese, L., Kennicutt, R. C., & Saha, A. 2004, *ApJ*, 608, 42
- Scowcroft, V., Bersier, D., Mould, J. R., & Wood, P. R. 2009, *MNRAS*, 396, 1287
- Seaton, M. J. 1979, *MNRAS*, 187, 73P
- Simón-Díaz, S., & Stasińska, G. 2010, *ArXiv e-prints*
- Stanghellini, L., Magrini, L., Villaver, E., & Galli, D. 2010, *A&A*, 521, A3
- Tammann, G. A., Sandage, A., & Reindl, B. 2008, *ApJ*, 679, 52
- Thim, F., Tammann, G. A., Saha, A., Dolphin, A., Sandage, A., Tolstoy, E., & Labhardt, L. 2003, *ApJ*, 590, 256
- Tremonti, C. A., et al. 2004, *ApJ*, 613, 898
- Trundle, C., Dufton, P. L., Lennon, D. J., Smartt, S. J., & Urbaneja, M. A. 2002, *A&A*, 395, 519
- Trundle, C., & Lennon, D. J. 2005, *A&A*, 434, 677
- Tsamis, Y. G., Barlow, M. J., Liu, X., Danziger, I. J., & Storey, P. J. 2003, *MNRAS*, 338, 687
- Turner, D. G. 2010, *Ap&SS*, 326, 219
- U, V., Urbaneja, M. A., Kudritzki, R.-P., Jacobs, B. A., Bresolin, F., & Przybilla, N. 2009, *ApJ*, 704, 1120
- van Albada, G. D. 1980, *A&A*, 90, 123
- van Leeuwen, F., Feast, M. W., Whitelock, P. A., & Laney, C. D. 2007, *MNRAS*, 379, 723
- Vila-Costas, M. B., & Edmunds, M. G. 1992, *MNRAS*, 259, 121
- Webster, B. L., & Smith, M. G. 1983, *MNRAS*, 204, 743
- Zaritsky, D., Kennicutt, Jr., R. C., & Huchra, J. P. 1994, *ApJ*, 420, 87

APPENDIX

A. METALLICITIES OF CEPHEID HOST GALAXIES IN THE T_e SCALE

In this Appendix the oxygen abundances of Cepheid host galaxies are calculated self-consistently, using (a) observations of the [O III] $\lambda 4363$ auroral line or (b) the conversion given in Eq. 3 between abundances obtained from the Zaritsky et al. (1994, ZKH) calibration of R_{23} and T_e -based abundances. This equation was obtained by comparing upper branch abundances for a large sample of H II regions measured using the two methods. It should be recalled that the ZKH calibration only holds for the metal-rich branch of R_{23} , and therefore the transformation is not defined for the low-metallicity branch ($12 + \log(O/H)_{T_e} < 8$).

Table 7
Cepheid host irregular galaxies with [O III] $\lambda 4363$ detections

Galaxy	$12 + \log(\text{O}/\text{H})$	Sources of emission line data
LMC	8.36 ± 0.10	Dufour (1975); Pagel et al. (1978); Dufour et al. (1982) Russell & Dopita (1990); Tsamis et al. (2003)
SMC	8.03 ± 0.09	Dufour (1975); Dufour & Harlow (1977); Pagel et al. (1978) Russell & Dopita (1990); Tsamis et al. (2003)
IC 1613	7.78 ± 0.05	Bresolin et al. (2007)
WLM	7.82 ± 0.08	Lee et al. (2005)
NGC 3109	7.79 ± 0.08	Peña et al. (2007)
NGC 6822	8.12 ± 0.07	Lee et al. (2006)
Sextans A	7.48 ± 0.02	Kniazev et al. (2005)
Sextans B	7.59 ± 0.20	Kniazev et al. (2005)
NGC 5253	8.20 ± 0.03	Kobulnicky et al. (1997); López-Sánchez et al. (2007)

Table 8
Cepheid host spiral galaxies with [O III] $\lambda 4363$ detections

Galaxy	$12 + \log(\text{O}/\text{H})_{T_e}$	Sources of emission line data
M33 (inner) ¹	8.39 ± 0.04	Bresolin et al. (2010)
M33 (outer) ¹	8.26 ± 0.07	Bresolin et al. (2010)
M101 (inner) ²	8.64 ± 0.06	Kennicutt et al. (2003); Bresolin (2007)
M101 (outer) ²	8.26 ± 0.08	Kennicutt et al. (2003); Bresolin (2007)
NGC 300	8.33 ± 0.13	Bresolin et al. (2009)
NGC 2403	8.28 ± 0.11	Garnett et al. (1997)

¹ Scowcroft et al. (2009)

² Kennicutt et al. (1998)

A.1. Irregular and dwarf galaxies with abundances determined from [O III] $\lambda 4363$ detections.

Emission line data for nine irregular and dwarf galaxies with [O III] $\lambda 4363$ line detections were drawn from the literature, and the oxygen abundances for individual H II regions were calculated using the same method (IRAF's `temden` and `ionic` routines) and atomic data (see Bresolin et al. 2009 for details) used for our T_e -based abundance determinations in NGC 4258. The average abundances and standard deviations are reported in Table 7, together with the literature sources for the emission line data.

A.2. Spiral galaxies with abundance gradients determined from [O III] $\lambda 4363$ detections.

Four spiral galaxies with a well-determined oxygen abundance gradient based on the detection of [O III] $\lambda 4363$ are presented in Table 8. Cepheids in two fields at different galactocentric distances have been observed in M33 (Scowcroft et al. 2009) and M101 Kennicutt et al. (1998). The abundances in the inner and outer fields of M33 and M101 were calculated from the following expressions for the abundance gradients:

$$M33: 12 + \log(\text{O}/\text{H}) = 8.42 (\pm 0.03) - 0.26 (\pm 0.07) R/R_{25}, \text{ with } R_{25} = 35'.4 \text{ (Bresolin et al. 2010).}$$

$$(R_{\text{inner}} = 3'.6, R_{\text{outer}} = 21'.1)$$

$$M101: 12 + \log(\text{O}/\text{H}) = 8.75 (\pm 0.05) - 0.90 (\pm 0.07) R/R_{25}, \text{ with } R_{25} = 14'.4 \text{ (Bresolin 2007).}$$

$$(R_{\text{inner}} = 1'.7, R_{\text{outer}} = 7'.9)$$

The Cepheids studied in NGC 300 cover a wide range in radius, and one could crudely divide them into an inner and an outer sample, using the following expression for the abundance gradient:

$$NGC 300: 12 + \log(\text{O}/\text{H}) = 8.57 (\pm 0.02) - 0.41 (\pm 0.03) R/R_{25}, \text{ with } R_{25} = 9'.75 \text{ (Bresolin et al. 2009).}$$

The oxygen abundance for NGC 300 in Table 8 is the average for H II regions at galactocentric distances larger than $0.3 R_{25}$, where the bulk of the Cepheids is located. In the case of NGC 2403 the abundances of the five H II regions from Garnett et al. (1997) at galactocentric distances larger than 2.7 kpc ($0.25 R_{25}$) were averaged.

A.3. Oxygen abundances for Cepheid host galaxies using the transformation to the T_e scale

For galaxies in which no (or only a few) [O III] $\lambda 4363$ line detections are available we used Eq. 3 to scale the oxygen abundances calculated in the ZKH scale to the T_e scale. The results are presented in Table 9. The galaxy list was drawn from Sakai et al. (2004), Saha et al. (2006) and Bono et al. (2010), with the addition of a few galaxies. Unless otherwise noted (see references at the end of the table), the abundances in the ZKH scale were taken from Ferrarese et al. (2000).

We comment below on a few galaxies from Table 9 in which auroral lines have been detected:

NGC 224 (M31): A value of $12 + \log(\text{O}/\text{H}) = 8.41 \pm 0.02$ has been reported by Esteban et al. (2009) from a detection of [O III] $\lambda 4363$ in the outlying H II region K932 ($R \simeq 16$ kpc from the galaxy center). Given the rather shallow abundance gradient in this galaxy (still uncertain, but between -0.006 and -0.027 dex kpc^{-1} , Trundle et al. 2002), this direct T_e -based abundance is probably a good measurement of the overall metallicity.

NGC 1365: Bresolin et al. (2005) measured chemical abundances from the [N II] $\lambda 5755$, [S III] $\lambda 6312$ and [O II] $\lambda 7325$ auroral lines for three H II regions in the vicinities of the Cepheids studied by the *HST* Key Project. The weighted mean oxygen abundance is $12 + \log(\text{O}/\text{H}) = 8.48 \pm 0.10$, in good agreement with the value of 8.48 given in Table 9 for the T_e scale.

NGC 3031 (M81): The detection of [O III] $\lambda 4363$ in H II regions in the galactocentric radial range 5.8-9.8 kpc has been reported by Stanghellini et al. (2010). The average abundance they derived is $12 + \log(\text{O}/\text{H}) = 8.54^{+0.18}_{-0.32}$. This metallicity should be representative of the inner field in Table 9, which gives a lower value of 8.33.

NGC 5236 (M83): Bresolin et al. (2005) measured chemical abundances from the [N II] $\lambda 5755$, [S III] $\lambda 6312$ and [O II] $\lambda 7325$ auroral lines for two H II regions in the vicinities of the Cepheids studied by Thim et al. (2003). The weighted mean oxygen abundance is $12 + \log(\text{O}/\text{H}) = 8.55 \pm 0.10$, in good agreement with the value of 8.64 given in Table 9.

NGC 7793: From the emission line data published by Edmunds & Pagel (1984) for two H II regions with good [O III] $\lambda 4363$ detection we derive $12 + \log(\text{O}/\text{H}) = 8.42 \pm 0.09$, in agreement with the 8.45 value in Table 9.

Table 9
Metallicities of other Cepheid host galaxies in the T_e and ZKH scales

Galaxy	$12 + \log(\text{O}/\text{H})$		error
	T_e scale	ZKH scale	
NGC 55	8.06	8.35 ^a	0.15
NGC 224	8.49	8.98	0.15
NGC 925	8.19	8.55	0.15
NGC 1309	8.44	8.90 ^b	0.19
NGC 1326A	8.16	8.50	0.15
NGC 1365	8.48	8.96	0.20
NGC 1425	8.50	9.00	0.15
NGC 1637	8.56	9.08 ^c	0.15
NGC 2090	8.37	8.80	0.15
NGC 2541	8.16	8.50	0.15
NGC 2841	8.71	9.30 ^d	0.15
NGC 3021	8.46	8.94 ^b	0.25
NGC 3031 (inner) ¹	8.33	8.75	0.15
NGC 3031 (outer) ²	8.23	8.60 ^e	0.15
NGC 3198	8.23	8.60	0.15
NGC 3319	8.08	8.38	0.15
NGC 3351	8.67	9.24	0.20
NGC 3368	8.64	9.20	0.20
NGC 3370	8.37	8.80 ^f	0.19
NGC 3621	8.33	8.75	0.15
NGC 3627	8.68	9.25	0.15
NGC 3982	8.33	8.75 ^f	0.25
NGC 4321	8.59	9.13	0.20
NGC 4414	8.64	9.20	0.15
NGC 4496A	8.35	8.77	0.15
NGC 4527	8.33	8.75 ^g	0.15
NGC 4535	8.64	9.20	0.15
NGC 4536	8.40	8.85	0.15
NGC 4548	8.74	9.34	0.15
NGC 4639	8.50	9.00	0.15
NGC 4725	8.45	8.92	0.15
NGC 5236	8.64	9.20 ^h	0.15
NGC 7331	8.28	8.67	0.15
NGC 7793	8.45	8.92 ⁱ	0.12
IC 4182	8.09	8.40	0.20

References. — (a) Zaritsky et al. (1994); (b) Riess et al. (2009a); (c) Leonard et al. (2003); (d) using line fluxes from Bresolin et al. (1999); (e) McCommas et al. (2009) (f) Riess et al. (2005); (g) Saha et al. (2006); (h) using line fluxes from Bresolin et al. (2005); (i) using line fluxes from Webster & Smith (1983)

¹ Freedman et al. (1994)

² McCommas et al. (2009)